RESEARCH ARTICLE

Key Points:
- Model/observation study of 26.5°N Atlantic heat transport at 5 day to monthly timescales
- Contrasting wind field patterns drive transport variability at the two timescales considered
- North-westerly winds from North America drive 5 day variability and reduce transport by 0.5–1.4 PW

Correspondence to:
B. I. Moat,
bim@noc.ac.uk

Major variations in subtropical North Atlantic heat transport at short (5 day) timescales and their causes

B. I. Moat[1], S. A. Josey[1], B. Sinha[1], A. T. Blaker[1], D. A. Smeed[1], G. D. McCarthy[1], W. E. Johns[2], J. J.-M. Hirschi[1], E. Frajka-Williams[3], D. Rayner[1], A. Duchez[1], and A. C. Coward[1]

[1]National Oceanography Centre, University of Southampton, Southampton, UK, [2]Rosentiel School of Marine and Atmospheric Science, University of Miami, Miami, Florida, USA, [3]Ocean and Earth Science, National Oceanography Centre, University of Southampton, Southampton, UK

Abstract Variability in the North Atlantic ocean heat transport at 26.5°N on short (5 day) timescales is identified and contrasted with different behaviour at monthly intervals using a combination of RAPID/MOCHA/WBTS measurements and the NEMO-LIM2 1/12° ocean circulation/sea ice model. Wind forcing plays the leading role in establishing the heat transport variability through the Ekman transport response of the ocean and the associated driving atmospheric conditions vary significantly with timescale. We find that at 5 day timescales the largest changes in the heat transport across 26.5°N coincide with north-westerly airflows originating over the American land mass that drive strong southward anomalies in the Ekman flow. During these events the northward heat transport reduces by 0.5–1.4 PW. In contrast, the Ekman transport response at longer monthly timescales is smaller in magnitude (up to 0.5 PW) and consistent with expected variations in the leading mode of North Atlantic atmospheric variability, the North Atlantic Oscillation. The north-westerly airflow mechanism can have a prolonged influence beyond the central 5 day timescale and on occasion can reduce the accumulated winter ocean heat transport into the North Atlantic by ∼40%.

1. Introduction

The Atlantic Meridional Overturning Circulation (AMOC) is a key component of the global ocean circulation and contributes to the comparatively mild climate of Western Europe. Indeed, a large fraction of the heat released to the atmosphere by the AMOC is carried eastward by the predominant westerly winds, leading to warmer temperatures in northwestern Europe than at similar latitudes in eastern Canada [*Rhines et al.*, 2008; *Sinha et al.*, 2012].

Variations in the wind forcing of the ocean play a significant role in modifying the strength of the AMOC across a range of timescales from seasonal to interannual [*Zhao and Johns*, 2014a, 2014b]. At annual timescales, *Stepanov and Haines* [2014] have also recently shown that the AMOC transport substantially depends upon the strength of the wind. They found that weaker zonal winds over the North Atlantic lead to an increase in the AMOC using a $1/4°$ resolution Ocean General Circulation Model (OGCM). At longer interannual timescales, strong winds over the Subpolar Gyre lead to an increase in the AMOC by means of an increase in the deep water formation in the North Atlantic Subpolar Gyre.

At monthly to annual time scales, there is evidence from observations and models for large anomalies in the AMOC strength arising mainly from wind-forced variability [*Bryden et al.*, 2014; *Blaker et al.*, 2015; *McCarthy et al.*, 2012; *Cunningham et al.*, 2013; *Roberts et al.*, 2013; *Zhao and Johns*, 2014a, 2014b] with a contribution from ocean internal variability [*Hirschi et al.*, 2013; *Thomas and Zhai*, 2013]. During 2009–2010, a 30% slowdown in the AMOC was observed in measurements from the RAPID array at 26.5°N and resulted in a reduction in the northward ocean heat transport by 0.4 PW. It led to cooler upper ocean waters north of 26.5°N [*Sonnewald et al.*, 2013; *Bryden et al.*, 2014] that may have played a role in the subsequent severe winter in northwestern Europe. *Buchan et al.* [2014] used surface-forced atmosphere model experiments to show that North Atlantic SST anomalies in 2009–2010 were particularly conducive to the development of a negative NAO phase, which culminated in the extreme cold weather conditions experienced over northern Europe in winter 2010–2011.

Cunningham et al. [2013] showed that the cold anomalies are partly driven by anomalous air-sea exchange and partly by extreme interannual variability in the northward heat transport at 26.5°N. This variability in

the northward heat transport at 26.5°N results in cooling of the deeper layers isolated from the atmosphere on annual timescales. Subsequently this water is entrained into the winter mixed layer thus lowering winter sea surface temperatures. *Blaker et al.* [2015] demonstrated that both the $1/4°$ and $1/12°$ resolution NEMO OGCM forced with observed surface fluxes could reproduce the observed AMOC minimum during 2009–2010. They found three occasions in which pairs of AMOC minima events occurred in consecutive years (the 2009/2010 event and earlier in 1969/1970 and 1978/1979).

Shorter timescale (order 5 day) variability in the AMOC strength and the associated heat transport remains largely unexplored despite significant anomalies being evident in the RAPID array transport time series [*McCarthy et al.*, 2012]. Here we determine in detail for the first time the strength of heat transport variability at 26.5°N at 5 day timescales using observations from the array and output from a high resolution forced ocean model that captures much of the observed variability. We also establish the causes of the variability, identifying a previously unrecognized pattern of ocean-atmosphere coupling that drives strong zonally dependent variations in the heat transport.

Model comparison with observations over the recent RAPID decade of observations (April 2004 to March 2014) is used to first establish the reliability of the NEMO OCGM in estimating the heat transport across 26.5N. We then examine the model over longer multidecadal periods. The paper is organized as follows. Details of the RAPID heat transport measurements and the NEMO global ocean model are given in section 2. The results of our analysis are presented in section 3. The key issues are discussed in section 4.

2. Data Sets and Methodology

The RAPID array across 26.5°N has provided twice daily measurements of the AMOC and associated heat transport for 10 years (April 2004 to March 2014) [*Rayner et al.*, 2011; *Johns et al.*, 2011; *McCarthy et al.*, 2015; *Smeed et al.*, 2015]. The AMOC is constructed from a combination of a mooring array between the Bahamas and Africa, cable measurements of the Gulf Stream transport between Florida and the Bahamas [*Meinen et al.*, 2010], and Ekman transport calculated from the ERA interim wind field [*Dee et al.*, 2011].

The NEMO ORCA global ocean circulation model [*Madec*, 2008; *Marzocchi et al.*, 2015] version 3.6 is configured with 75 vertical z-levels ranging from 1 m at the surface to 250 m at 5500 m and a nominal resolution of $1/12°$. South of 20°N the model grid is isotropic Mercator, and north of 20°N the grid becomes quasi-isotropic bipolar, with poles located in Canada and Siberia to avoid numerical instability associated with convergence of the meridians at the geographic North Pole. At 26.5°N the resolution is approximately 8.3 km, becoming finer at higher latitudes such that at 60°N/S it becomes 4.6 km. Bottom topography is represented as partial steps and bathymetry is derived from ETOPO2 [*U.S. Department of Commerce*, 2006]. Climatological initial conditions for temperature and salinity were taken in January from PHC2.1 [*Steele et al.*, 2001] at high latitudes, MEDATLAS [*Jourdan et al.*, 1998] in the Mediterranean, and *Levitus et al.* [1998] elsewhere. It is forced by the Drakkar Surface Forcing data set version 5.2, which supplies surface air temperature, winds, humidity, surface radiative heat fluxes and precipitation, and is integrated for the period 1958–2012 [*Dussin et al.*, 2014; *Brodeau et al.*, 2010]. To prevent excessive drifts in global salinity due to deficiencies in the fresh water forcing, sea surface salinity is relaxed toward climatology with a piston velocity of 33.33 mm/day/psu. Sea ice is represented by the Louvain-la-Neuve Ice Model version 2 (LIM2) sea-ice model [*Timmerman et al.*, 2005].

The model meridional heat transport is computed by integrating the product of the meridional velocity and temperature across 26.5°N. The meridional heat transport value is based on an assumed zero net transport through the section, whereas there is actually a net transport of ∼1.0 Sv through the basin resulting from the Bering Strait throughflow to the Arctic. Balancing this flow in the model meridional heat transport calculation introduces an additional small correction [e.g., *Hall and Bryden*, 1982] to the southward heat transport of order −0.03 PW. For comparison with RAPID observations the model heat transport is split into different temperature transport components as follows (after *Johns et al.* [2011]):

$$Q_{NET} = Q_{FS} + Q_{EK} + Q_{MO} + Q_{WBW} + Q_{EDDY} \tag{1}$$

In the above, Q_{FS} is the Florida Straits temperature transport, Q_{WBW} is the western boundary wedge temperature transport over the Bahamian shelf (between the Bahamas and the location of a RAPID array tall mooring at (26.52°N, 76.74°W) referred to as WB2), Q_{EK} is the Ekman temperature transport over the mid-ocean
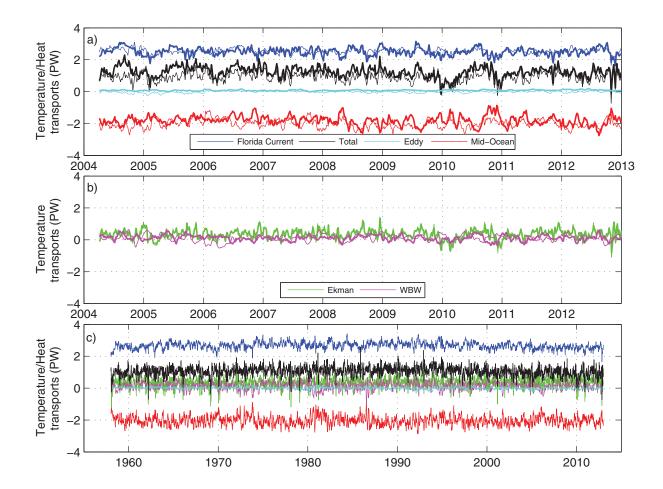
Figure 1. 5 day mean temperature transports (relative to 0°C), for each of the contributions to the net meridional heat transport at 26.5°N: (a, b) model (thin) and RAPID (bold) for 2004–2012; and (c) model time series between 1958 and 2012.

region (between WB2 and Africa), Q_{MO} is the zonally averaged contribution of the mid-ocean temperature transport and Q_{EDDY} is the mid-ocean eddy contribution due to spatially correlated velocity and temperature fluctuations. Temperature transports are defined as transports relative to a reference of 0°C. Q_{EDDY} is actually a true heat transport as it has no mass transport associated with it and is independent of temperature reference; as is the net meridional heat transport. The model derived value for Q_{MO} differs slightly from that calculated using RAPID as it was determined by integration of the spatially complete model velocity and temperature fields, rather than using a geostrophic calculation across the mid-ocean region as is the case for the observed value. To make this consistent with observations, the model Ekman and eddy fields were removed from the Q_{MO}.

Five day and monthly average heat transport time series to be discussed in section 3.1 each show strong variability. In order to identify the cause of the strongest events a composite analysis of the 10 strongest positive and 10 strongest negative events was performed for both the 5 day and monthly averaged data.

3. Results

3.1. Evaluation of NEMO Heat Transport Using RAPID Array Measurements

The model heat transport averaged over 5 day intervals is decomposed into the RAPID components (Table 1) and compared with observations in Figure 1. The tabulated values reveal that the model mean Florida Current and western boundary wedge (WBW) temperature transports are in close agreement with the observations. For the Florida Current, the model/observation-based values are 2.54/2.50 PW, while for

Table 1. Mean Values and Standard Deviations From 5 Day Averages of Model and Observed Temperature Transport Components for the Period 2004 to the End of 2012[a]

Meridional Temperature Transport Component	1/12° NEMO	RAPID
Florida Straits	2.54 ± 0.16	2.50 ± 0.25
Ekman (WB2 to Africa)	0.34 ± 0.31	0.35 ± 0.30
Mid-Ocean (WB2 to Africa)	−2.02 ± 0.27	−1.81 ± 0.31
Western Boundary -Abaco	0.12 ± 0.21	0.12 ± 0.18
Eddy (WB2 to Africa)	−0.02 ± 0.06	0.08 ± 0.03
Total temperature transport	0.96 ± 0.32	1.24 ± 0.35
Total Heat transport	0.93 ± 0.32	1.24 ± 0.36

[a]The total heat transport is a mass compensated heat transport. Units of PW (10^{15} W).

the WBW both model and observations give a value of 0.12 PW. The eddy transport is slightly underestimated by the model (−0.02/0.08 PW), but the contribution of this term to the total heat transport is the smallest of the five components. As expected, the Ekman transport values are very close (0.34/0.35 PW) as similar wind fields are used for forcing the model and in the RAPID analysis.

Turning to the remaining component, the model value (−2.02 PW) for the southward flowing mid-ocean transport is a little stronger than the observed value (−1.81 PW). Consequently, the total heat transport from the model (0.93 PW) is about 0.3 PW less than the RAPID value (1.24 PW). However, the level of variability is similar in each case with standard deviation values of 0.31/0.37 PW derived from the model/observations. The correlation coefficient for the regression between the RAPID heat transport and the total model heat transport is 0.77(0.73) for the 5 day(monthly) values. Furthermore, the time series typically show good agreement with, for example, the reduction in the AMOC during the 2009/2010 period [*McCarthy et al.*, 2012] being well reproduced by the model. Thus, the model is expected to be a useful tool for identifying the key mechanisms responsible for heat transport variability at 26°N.

The long period spanned by the model run (1958–2012) provides an indication of whether the level of variability seen in the RAPID decade is maintained over the preceding 45 years (Figure 1c). This is seen to be the case with similar variability in each component and the total transport across the full period considered and no obvious inter-decadal changes. The model extremes in heat transport vary from a peak of 2.6 PW in 1985 to near zero and even negative values (e.g., 1962, 1969, 1978, 1979, 1998, 2009, 2010, 2012). In the next section, a composite analysis is employed to determine the oceanic and atmospheric conditions that give rise to such extreme values of the heat transport.

3.2. Driving Mechanisms for Heat Transport Extremes

The main focus of our analysis is the recent period from 1985 onward as the model forcing fields are likely to be better constrained in this period due to the advent of satellite observations for assimilation into the reanalysis on which they are based. We thus consider two model decades 1985–1994 and 1995–2004, as well as the RAPID decade 2004–2014. Five day and monthly average heat transport time series from the model for 1985–1994 and 1995–2004 are shown in Figures 2a and 2b, and from the RAPID observations for 2004–2014 in Figure 2c). The climatological mean seasonal cycle calculated for each decade has been removed from each time series. Figure 2d) shows a direct comparison between RAPID and model in the overlap period from 2004 to 2012. The climatological mean seasonal cycle calculated for the 8 year period has been removed from the time series.

The 10 strongest positive and negative heat transport anomalies were identified for both the 5 day and monthly extremes in each decade and are indicated by symbols in Figure 2; they predominantly occur in winter (October to March). The standard deviation of the heat transport for the two model decades using 5 day averages (monthly averages) is 0.26 (0.15) PW for 1985–1994 and 0.27 (0.17) PW for 1995–2004, i.e., a similar level of variability between decades. The corresponding standard deviation from the observations over the RAPID decade is 0.31 (0.23) PW, which is similar in level to the model for the earlier decades again indicating that the model has a realistic representation of the typical strength of the short-term variability in each 10 year time span.

The typical magnitude of the model and RAPID extreme transport anomalies has been considered for the 8 year period 2004–2012 in which they overlap by selecting the eight strongest positive and negative anomalies (note eight values are selected rather than 10 previously because the overlap does not span a full decade Figure 2d). The mean ± standard deviation of the eight strongest positive anomalies is similar in the model (0.68 ± 0.12 PW) and observations (0.76 ± 0.18 PW). Good agreement is also found for the negative events for which the corresponding values are (−0.81 ± 0.23 PW) for the model and (−0.75 ± 0.34 PW) for the observations. Thus, in both the positive and negative anomaly cases the model anomalies are of similar
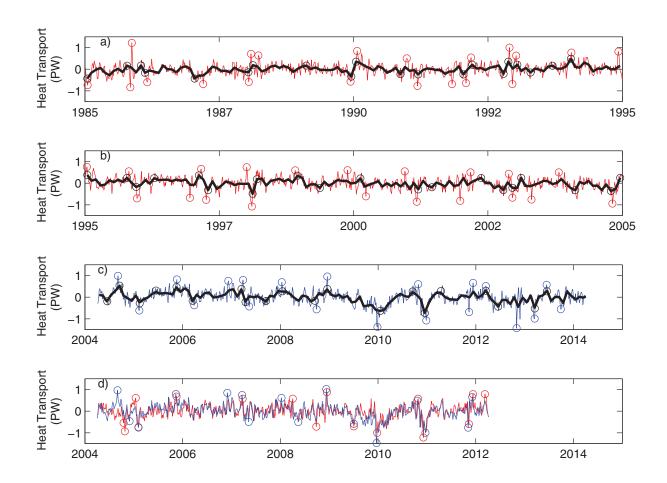
Figure 2. Time series of the model heat transport for the period (a) 1985–1994 and (b) 1995–2004 for 5 day averages (red) and monthly averages (black). RAPID heat transport measurements (5 day blue, monthly black) across 26.5°N are shown in (c) 2004–2014. (d) Model (red) and RAPID (blue) heat transport time series are shown for the overlap period 2004–2012 . The symbols indicate the 10 strongest positive and negative events in each decade and are shown for both the 5 day and monthly series. The climatological mean has been removed from all time series.

amplitude to those observed indicating its suitability for further analysis of these events. Considering the complete time series for the overlapping period, the standard deviation of the model (RAPID) heat transport is 0.31 (0.35) PW. So, in summary, the model reproduces the observed 5 day timescale variability well both in terms of the strength of the extreme events and the typical level of variability.

Histograms of the 5 day timescale model heat transport anomalies for 1985–1994, 1995–2004, and the RAPID decade (2004–2014) are shown in Figure 3. The distributions of the anomalies in each decade have a broadly symmetric distribution. The strongest positive and negative events are indicated and their means are similar in each decade: 1985–1994 (−0.68/0.76 PW), 1995–2004 (−0.79/0.59 PW) and RAPID (−0.81/0.73 PW).

We consider the first two decades (1985–1994) and (1995–2004) in our study period to begin with and then focus on the RAPID decade. Composite maps showing the vector wind stress (arrows) and the anomaly of the magnitude of the wind stress (colored field) averaged over the strongest positive and negative monthly events for 1985–1994 are shown in Figure 4. During the strongest positive events the wind stress pattern is typical of a North Atlantic Oscillation (NAO) positive state with enhanced westerly wind stress at about 50°N. The strongest negative events are typical of an NAO negative state with reduced wind stress at the same latitude.

The anomaly composite fields for the strongest positive and negative 5 day events for 1985–1994 are shown in Figure 5. At these shorter time scales, the pattern of the wind stress anomaly for the strongest positive events (Figure 5a) is broadly similar to the monthly events although stronger in magnitude
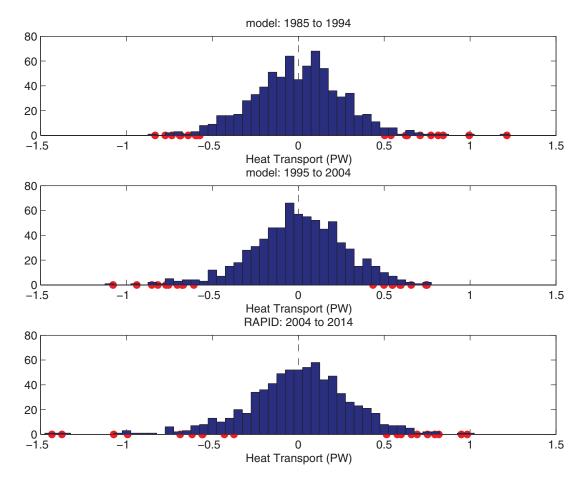
Figure 3. Histograms of the 5 day heat transport anomalies across 26.5°N for each decade considered in the text. The dots indicate the strong positive and negative events selected for the composite analysis.

(Figure 4a), with enhanced wind stress between 50 to 60°N and south of the RAPID array line at 26.5°N. However, the pattern for the extreme negative events at 5 day time scales differs significantly from that at monthly timescales and has not to our knowledge been documented elsewhere. It is dominated by strong north to north-westerly winds blowing off the American land mass which occur predominantly in winter. This leads to enhanced wind stress close to the American east coast, a change in direction of the mean wind field and a reversal in the Ekman transport at 26.5°N. The spatial pattern associated with the extreme negative anomalies is broadly similar in the subsequent decades with the main feature being anomalous north-westerly flow from the American land mass (Figures 6a and 6b). Likewise, similar patterns are obtained in the earlier decades 1965–1974 and 1975–1984 (not shown).

The Ekman transport across 26.5°N for the monthly and 5 day positive and negative composites is shown in Figure 7. During the 10 strongest monthly positive event composites the Ekman transport is northward across the full longitude range in each decade (Figure 7, left). This leads to an increase in the heat transport of up to 0.5 PW (Figure 2a). The corresponding monthly negative event composites shows a near zero Ekman transport in the west increasing to a small northward transport close to the African coast.

At 5 day time scales (Figure 7, right), the Ekman transport for the positive event composite is stronger than at monthly time scales. It is fairly uniform across the 26.5°N section and corresponds to an increase in heat transport of 0.5–1.2 PW (Figure 2a). In contrast, the Ekman transport for the 5 day negative event composites is southward. There is a marked zonal asymmetry in the Ekman transport for the 5 day negative event composites in the 1985–1994 decade (Figure 7b). Specifically, the Ekman transport is southward in the western section of 26.5°N and close to zero across the eastern section. This reversal of the Ekman transport in
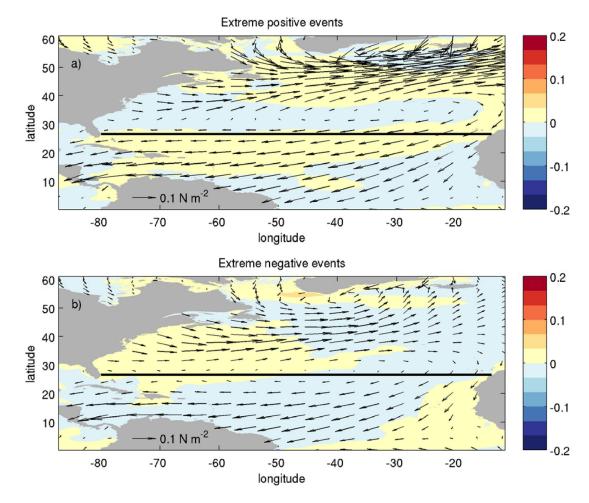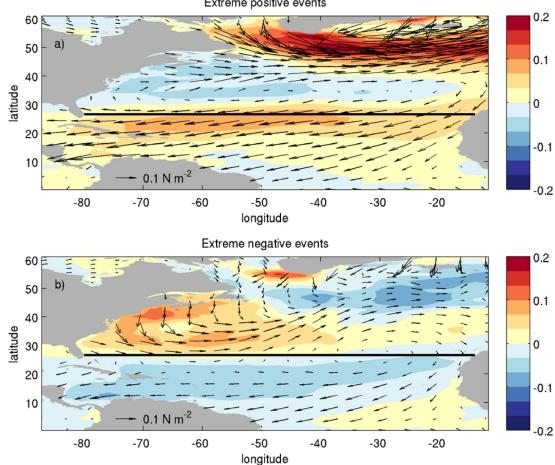
Figure 4. Model monthly averaged wind stress anomaly for (a) the 10 extreme positive events and (b) 10 extreme negative events between 1985 and 1994. The arrows show the mean wind stress averaged over the 10 events. The solid lines indicate the 26.5°N latitude of the RAPID section.
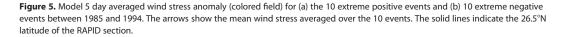
the west is due to the north-westerly winter wind outbreaks from the American land mass. The wind stress anomaly associated with the 5 day outbreak events was located further westward and southward during the 1995–2004 decade (Figure 6b), giving rise to a more symmetric southward Ekman transport across 26.5°N (Figure 7d). During the RAPID decade (2004–2014) the wind stress anomaly was of greater intensity than in/during the previous two decades (Figure 6b), but was not located as far south. At 26.5°N this resulted in a weaker southward Ekman transport with a weak asymmetry across the 26.5°N section. Integrated over the section, for the negative 5 day event composites the Ekman transport is southward and has magnitude 2.0 ± 2.3 Sv (1985–1994), 4.5 ± 3.1 Sv (1995–2004) and 3.1 ± 5.2 Sv (RAPID decade). This accounts for a reduction in the northward heat transport by 0.5–1.4 PW (Figures 2a–2c).

At short 5 day time scales the north-westerly winter outbreak events affect the wind stress pattern over the western and central Atlantic Ocean. This mechanism drives heat southward by means of a reversal in the mean wind field, which results in a reversal of the Ekman transport. These events are short duration in nature, consequently the negative monthly events (Figure 4b) do not show the same pattern as the negative 5 day events (Figure 5b). The effect on Ekman transport at 26N is similarly dependent on timescale. Negative monthly events have little impact on Ekman transport (Figure 7, left) whereas the negative 5 day events—particularly in the two decades 1985–1994 and 1995–2004—contribute to a reduction in the typically northward transport at 26N.

We close this section by noting that in future work we plan to carry out a spectral analysis to advance our understanding of the short-term meridional heat transport variability. This will provide further insights into

Figure 5. Model 5 day averaged wind stress anomaly (colored field) for (a) the 10 extreme positive events and (b) 10 extreme negative events between 1985 and 1994. The arrows show the mean wind stress averaged over the 10 events. The solid lines indicate the 26.5°N latitude of the RAPID section.
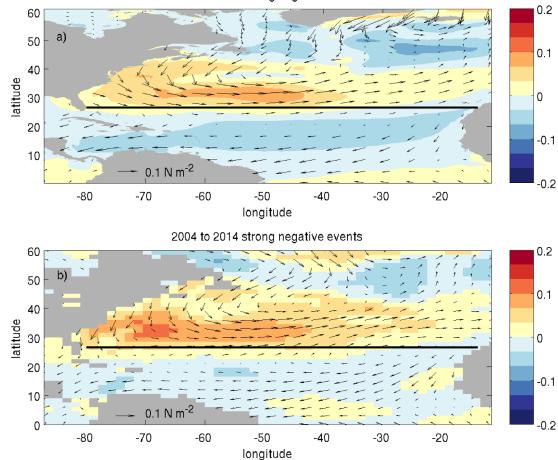
the statistical significance of our results and the nature of the underlying processes. For this follow-on study we will have access to higher frequency model output (6 hourly) from the next planned run of the model. At present we are limited to 5 daily output from the model run used in the analysis reported here.

3.3. Heat Transport Anomalies and Regional Climate
3.3.1. Air-Sea Exchanges

We now consider the short (5 day) timescale heat transport anomalies within the context of the regional climate, in particular the exchange of heat between the ocean and atmosphere. As the driving mechanism for the transport anomalies involves wind forcing of the ocean, we anticipate that there may also be an associated heat flux anomaly as the latent and sensible heat flux components of the net heat exchange are wind speed dependent. In particular, the latent (sensible) heat flux is largely determined by the product of wind speed and sea-air humidity gradient (sea-air temperature gradient).

Composite fields of the 5 day net heat exchange anomaly coincident in time with the 10 strongest positive and negative heat loss transport anomalies for 1985–1994 are shown in Figure 8. The composite associated with the strong negative heat transport events (Figure 8b) exhibits a broad region of enhanced heat loss across the western half of the Atlantic north of 26.5°N, reaching peak values of close to 300 Wm^{-2} anomalous ocean heat loss. This pattern is consistent with the enhanced heat loss that is expected to arise given the wind field in Figure 5b as the flow of cold air from the American continent brings stronger winds, and cold, dry air enabling greater latent and sensible heat loss. Thus, the atmospheric forcing associated with

Figure 6. Five day mean wind stress anomaly averaged over the 10 strong negative events for: (a) model results for the 1995–2004 decade and (b) the ERA Interim wind stress fields employed in the RAPID analysis during the 2004–2014 decade. The arrows show the mean wind stress for each of the 10 events. The solid lines indicate the 26.5°N latitude of the RAPID section.

the strong negative events has the potential to reinforce OHC anomalies as reduced northward heat transport is accompanied by increased surface heat loss. As a consequence, the implications for OHC anomalies are of greater significance than expected on the basis of heat transport variations alone. For comparison, the integrated surface net heat loss anomaly for the box shown in Figure 8b is 0.32 PW which compares with an Ekman heat transport anomaly out of the box of 0.38 PW i.e., both processes are likely to be important given their broadly similar magnitudes.

In contrast, the composite field associated with the strong positive transport events (Figure 8a) shows heat flux anomalies with a reversal in sign within the region indicated by the box adjacent to the 26.5°N line. So, such events are likely to be less important in setting OHC anomalies.

3.3.2. Persistence Timescales

Thus far we have investigated the atmospheric conditions associated with the peak 5 day anomalies achieved by the heat transport. We now show that these atmospheric conditions can persist with reduced amplitude over periods much longer than 5 days and result in extended periods where the meridional heat transport is anomalously high or low. For each extreme transport anomaly in the 1985–1994 decade we define a persistence timescale by computing the number of 5 day periods before the anomaly changes sign going forward in time from the peak, and adding the number of 5 day periods before the anomaly changes sign going backward in time. This persistence timescale is found to vary from as little as 10 days to as much as 3 months. Note that although the events have persistence beyond the 5 day peak of the transport anomaly they differ in terms of the forcing mechanism from the events selected on the basis of the transport anomaly over a full month as discussed earlier.
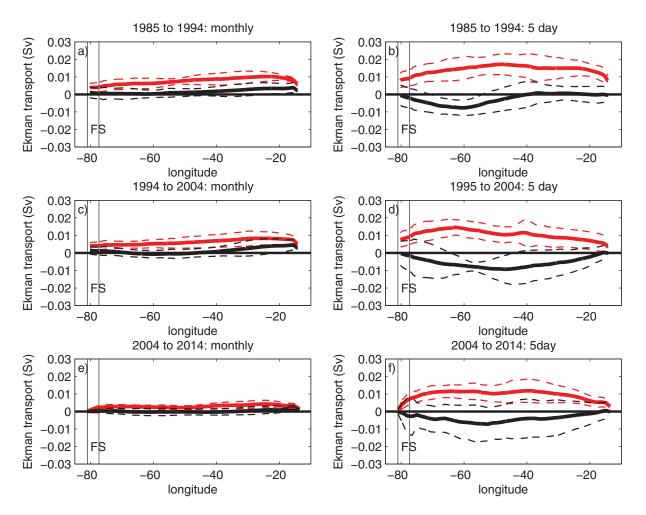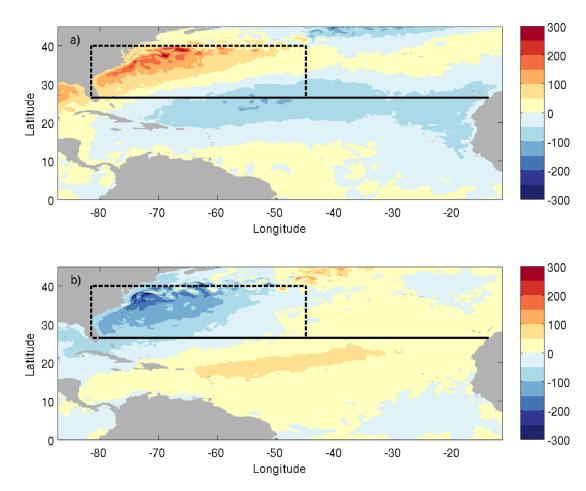
Figure 7. Ekman transport per kilometer across 26.5°N averaged over the (left) monthly and (right) 5 day positive (red) and negative events (black). The model estimates for two decades are shown: between (a, b) 1985 and 1994, and (c, d) 1995 and 2004. (e, f) The equivalent Ekman transport from the extremes identified in the RAPID heat transport time series are shown in for the period 2004–2014. The dashed lines indicate 1 standard deviation from the mean. The location of the Florida Straits is indicated by "FS."

We now form composite wind stress anomalies covering the persistence timescale assigned to each 5 day event (Figure 9) for the 1985–1994 decade. The composites based on the persistence timescale bear a striking resemblance to Figure 5 (based on single 5 day means rather than the persistence timescale), albeit with weaker amplitude. There is a clear difference with the composites based on monthly averages (Figure 4). The heat transport anomalies based on the extended events are lower than the peak extremes, but still substantial and are sustained over much longer periods in many cases. The mechanism highlighted in this paper is thus able to influence ocean heat transport over periods up to many weeks and on occasion can reduce the accumulated winter ocean heat transport into the North Atlantic by ~40%. The five strongest negative events reduce the transport by between 0.44 and 0.51 PW (about 40% of the total). Coupled with the associated increase in surface heat loss noted in section 3.3.1 above, the consequence of these events for North Atlantic SST, winter variability and extremes are potentially significant and warrants further investigation in subsequent studies.

4. Summary and Conclusions

The primary aim of this study is to examine the causes of heat transport variability across 26.5°N in the North Atlantic at relatively short (order 5 day) timescales that have been unexplored to date. A combination
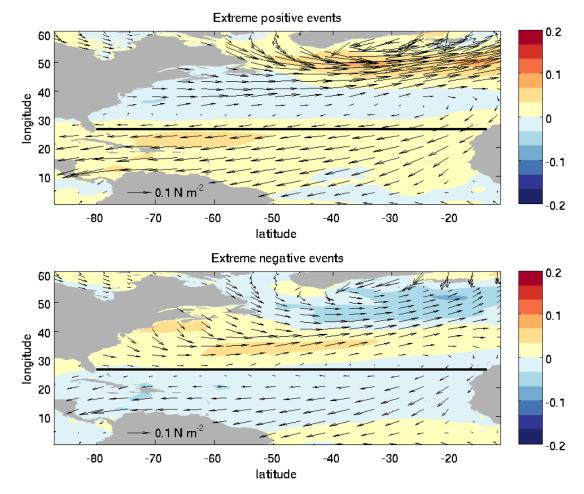
Figure 8. Composite fields of the net heat exchange (Q_{net}) anomaly coincident in time with the 10 strongest (a) positive and (b) negative heat loss transport anomalies in the 1985–1994 decade. Q_{net} is defined to be positive for heat gained by the oean from the atmosphere. The solid line indicate the 26.5°N latitude of the RAPID section, and the box shows the region used to determine area integrated heat flux anomaly in section 3.3.

of observations from the RAPID/MOCHA/WBTS array and output from the NEMO ORCA 1/12° ocean circulation model are used.

The RAPID components of the temperature transports [*Johns et al.*, 2011] were compared with the NEMO ocean circulation model. The model mean components compare well with observations, particularly the Florida Current and WBW temperature transports, although the model mid-ocean transport is a little stronger than observed. The level of heat transport variability is similar for model and observation-derived estimates with standard deviation values of 0.31 and 0.37 PW respectively. Furthermore, the time series typically show good agreement with, for example, the 2009/2010 reduction in the AMOC being well reproduced by the model. The typical magnitude of the large-amplitude, high-frequency events is well simulated by the model, making it a useful tool for investigating the mechanisms causing this heat transport variability

Using the model, we analyzed the difference in heat transport between decades with extreme positive and negative averaged heat transport anomalies at both 5 day and monthly time scales. This reveals large unexpected extremes in heat transport at short (5 day) time scales. At these 5 day time scales, north-westerly airflows originating over the American land mass drive strong southward anomalies in the Ekman flow across 26.5°N. These lead to a reduction in the northward heat transport by 0.5–1.4 PW. In contrast, the Ekman transport response at longer monthly timescales is smaller in magnitude (0.5 PW) and consistent with expected variations in the leading mode of North Atlantic atmospheric variability, the North Atlantic Oscillation.

Figure 9. Model averaged composite wind stress anomaly covering the persistence timescale assigned to each 5 day event for (a) the 10 extreme positive events and (b) 10 extreme negative events between 1985 and 1994. The arrows show the mean wind stress for each of the 10 events. The solid lines indicate the 26.5°N latitude of the RAPID section.

Composite fields of net heat flux exchange associated with the north-westerly airflows show a broad region of enhanced ocean heat loss across the western Atlantic North of 26.5°N. The atmospheric forcing associated with these events has the potential to have a reinforcing impact on Ocean Heat Content anomalies as reduced northward heat transport is accompanied by increased surface heat loss. These atmospheric conditions can persist over periods varying from as little as 10 days to as much as 3 months. Composites based on these times scales show the same mechanism as the shorter 5 day extremes and can reduce the winter ocean heat transport into the north Atlantic by up to 40%.

To conclude, we note that measurements of the AMOC from the RAPID array over the past decade have revealed a wide range of variability with the main focus being on timescales from monthly to interannual. Variability at short timescales has been relatively unexplored. Here we have shown using a combined model/observation analysis that the North Atlantic at 26.5° N exhibits significant heat transport variability at 5 day intervals and that this variability is controlled in part by a previously unrecognized mechanism involving the Ekman response of the ocean to anomalous north-westerly airflows from the American land mass. Similar processes are likely to be important elsewhere in the Atlantic, and other ocean basins, and we expect our analysis to inform future studies of short-term variability in ocean heat transports.

References

Blaker, A. T., J. J.-M. Hirschi, G. McCarthy, B. Sinha, S. Taws, R. Marsh, A. Coward, and B. de Cuevas (2015), Historical analogues of the recent extreme minima observed in the Atlantic meridional overturning circulation at 26N, *Clim. Dyn.*, *44*, 457–473, doi:10.1007/s00382-014-2274-6.

Brodeau, L., B. Barnier, A. M. Treguier, T. Penduff, and S. Gulev (2010), An ERA40-based atmospheric forcing for global ocean circulation models, *Ocean Modell.*, *31*, 88–104, doi:10.1016/j.ocemod.2009.10.005.

Bryden, H. L., B. A. King, G. McCarthy, and E. L. McDonagh (2014), Impact of a 30% reduction in Atlantic meridional overturning during 2009/2010, *Ocean Sci.*, *10*, 683–691, doi:10.5194/os-10-683-2014.

Buchan J., J. J.-M., Hirschi, A. T. Blaker, and B. Sinha (2014), North Atlantic SST Anomalies and the cold north European weather events of winter 2009-10 and December 2010, *Mon. Weather Rev.*, *142*, 922–932.

Cunningham, S. A., C. Roberts, W. E. Johns, W. Hobbs, E. Frajka-Williams, M. Palmer, G. McCarthy, D. Rayner, and D Smeed (2013), Atlantic meridional Overturning circulation slowdown cooled the subtropical ocean, *Geophys. Res. Lett.*, *40*, 6202–6207, doi:10.1002/2013GL058464.

Dee, D. P., et al. (2011), The ERA-Interim reanalysis: Configuration and performance of the data assimilation system, *Q. J. R. Meteorol. Soc.*, *137*, 553–597, doi:10.1002/qj.828.

Dussin, R., B. Barnier, and L. Brodeau (2014), The making of Drakkar forcing set DFS5, *DRAKKAR/MyOcean Rep. 05-10-14*, LGGE, Grenoble, France.

Hall, M. M., and H. L. Bryden (1982), Direct estimates and mechanisms of ocean heat transport, *Deep Sea Res., Part A*, *39*(3), 339–359.

Hirschi, J. J.-M., A. T. Blaker, B. Sinha, A. Coward, B. de Cuevas, S. Alderson, and G. Madec (2013), Chaotic variability of the meridional overturning circulation on subannual to interannual time scales, *Ocean Sci.*, *9*, 805–823, doi:10.5194/os-0-805-2013.

Johns, W. E., et al. (2011), Continuous, array-based estimates of Atlantic ocean heat transport at 26.5°N, *J. Clim.*, *24*, 2429–2449, doi:10.1175/2010JCLI3997.1.

Jourdan, D., E. Balopoulos, M. Garcia-Fernandez, and C. Maillard (1998), Objective analysis of temperature and salinity historical data set over the mediterranean basin, in *OCEANS'98 Conference Proceedings*, vol. 1, pp. 82–87, IEEE, Nice, France, doi:10.1109/OCEANS.1998.725649.

Levitus, S., M. Conkright, T. P. Boyer, T. O'Brian, J. Antonov, C. Stephens, L. S. D. Johnson and R. Gelfeld (1998), World ocean database 1998, *Tech. Rep. NOAA Atlas NESDIS 18*, U.S. Government Printing Office, Washington, D. C.

Madec, G. (2008), *NEMO Ocean Engine, Note du Pole de Modélisation*, vol. 27, 1288–1619, Inst. Pierre-Simon Laplace, Paris, France.

Marzocchi, A., J. J.-M. Hirschi, N. P. Holiday, S. A. Cunningham, A. T. Blaker, and A. Coward (2015), The North Atlantic subpolar circulation in an eddy-resolving global ocean model, *J. Mar. Syst.*, *142*, 126–143, doi:10.1016/j.jmarsys.2014.10.007.

McCarthy, G. D., E. Frajka-Williams, W. E. Johns, M. O. Baringer, C. S. Meinen, H. L. Bryden, D. Rayner, A. Duchez, C. D. Roberts, and S. A. Cunningham (2012), Observed interannual variability of the Atlantic meridional Overturning circulation at 26.5N, *Geophys. Res. Lett.*, *39*, L19609, doi:10.1029/2012GL052933.

McCarthy, G. D., D. A. Smeed, W. E. Johns, E. Frajka-Williams, B. I. Moat, D. Rayner, M. O. Baringer, C. S. Meinen, J. Collins, and H. L. Bryden (2015), Measuring the Atlantic Meridional Overturning Circulation at 26°N, *Prog. Oceanogr.*, *130*, 91–111, doi:10.1016/j.pocean.2014.10.006.

Meinen, C. S., M. O. Baringer, and R. F. Garcia (2010), Florida Current transport variability: An analysis of annual and longer period signals, *Deep Sea Res., Part I*, *57*, 835–846.

Rayner, D., et al. (2011), Monitoring the Atlantic meridional overturning circulation, *Deep Sea Res., Part II*, *58*, 1744–1753, doi:10.1016/j.dsr2.2010.10.056.

Rhines, P. B., S. Hakkinen, and S. A. Josey (2008), Is oceanic heat transport significant in the climate system?, in *Arctic-Subarctic Ocean Fluxes*, edited by R. Dickson, B. Hansen, and P. Rhines, chap. 4, pp. 87–110, Springer, Netherlands.

Roberts, C. D., et al. (2013), Atmosphere drives recent interannual variability of the Atlantic meridional overturning circulation at 26.5N, *Geophys. Res. Lett. 40*, 5164–5170, doi:10.1002/grl.50930.

Sinha, B., A. T. Blaker, J. J.-M. Hirsch, S. Bonham, M. Brand, S. A. Josey, R. Smith, and J. Marotzke (2012), Mountain ranges favour vigorous Atlantic meridional overturning, *Geophys. Res. Lett.*, *39*, L02705, doi:10.1029/2011GL05048.

Smeed, D. A., G. McCarthy, D. Rayner, B. I. Moat, W. E. Johns, M. O. Baringer, and C. S. Meinen (2015), *Atlantic Meridional Overturning Circulation Observed by the RAPID-MOCHA-WBTS (RAPID-Meridional Overturning Circulation and Heatflux Array-Western Boundary Time Series) Array at 26N From 2004 to 2014*, Br. Oceanogr. Data Cent., Liverpool, Nat. Environ. Res. Counc., U. K., doi:10/6qb.

Sonnewald, M., J. J-M Hirsch, R. Marsh, E. L. McDonagh, and B. A. King (2013), Atlantic meridional ocean heat transport at 26°N: Impact on subtropical ocean heat content variability, *Ocean Sci.*, *9*, 1057–1069, doi:10.5194/os-9-1057-2013.

Steele M, R. Morley, and W. Ermold (2001), PHC: A global ocean hydrography with a high quality Arctic Ocean, *J. Clim.*, *14*, 2079–2087.

Stepanov, V. N., and K. Haines (2014), Mechanisms of Atlantic Meridional Overturning Circulation variability simulated by the NEMO model, *Ocean Sci.*, *10*, 645–656, doi:10.519/os-10-645-2014.

Thomas, M. D., and X. Zhai (2013), Eddy-induced variability of the meridional overturning circulation in a model of the North Atlantic, *Geophys. Res. Lett.*, *40*, 2742–2747, doi:10.1002/grl.50532.

Timmerman A., H. Goosse, G. Madec, T. Fichefet, C. Ethe, and V. Dulire (2005), On the representation of high latitude processes in the ORCA-LIM global coupled sea-ice ocean model, *Ocean Modell.*, *8*, 175–201.

U.S. Department of Commerce (2006), U.S. Department of Commerce, National Oceanic and Atmospheric Administration, National Geophysical Data Center: 2-minute Gridded Global Relief Data (ETOPO2v2). [Available at http://www.ngdc.noaa.gov/mgg/global/etopo2.html.]

Zhao, J., and W. Johns (2014a), Wind-driven seasonal cycle of the Atlantic Meridional Overturning Circulation, *J. Phys. Oceanogr.*, *44*, 1541–1562, doi:10.1175/JPO-D-13-0144.1.

Zhao, J., and W. Johns (2014b), Wind-forced interannual variability of the Atlantic Meridional Overturning Circulation at 26.5°N, *J. Geophys. Res. Oceans*, *119*, 2403–2419, doi:10.1002/2013JC009407.